Neuroscience 268 (2014) 284–296

PROTEOMICS REVEAL ENERGY METABOLISM AND MITOGEN-ACTIVATED PROTEIN KINASE SIGNAL TRANSDUCTION PERTURBATION IN HUMAN BORNA DISEASE VIRUS HU-H1-INFECTED OLIGODENDROGLIAL CELLS

X. LIU,[a,b,c†] Y. YANG,[a,b,c†] M. ZHAO,[b,c†] L. BODE,[d†] L. ZHANG,[b,c†] J. PAN,[b,c] L. LV,[b,c] Y. ZHAN,[b,c] S. LIU,[b,c] L. ZHANG,[a,b,c] X. WANG,[b,c] R. HUANG,[b,c,e] J. ZHOU[b,c] AND P. XIE[a,b,c*]

[a] *Department of Neurology, The First Affiliated Hospital of Chongqing Medical University, Chongqing, China*

[b] *Chongqing Key Laboratory of Neurobiology, Chongqing Medical University, Chongqing, China*

[c] *Institute of Neuroscience, Chongqing Medical University, Chongqing, China*

[d] *Bornavirus Research Group affiliated to the Free University of Berlin, Berlin, Germany*

[e] *Department of Rehabilitation, The Second Affiliated Hospital of Chongqing Medical University, Chongqing, China*

Abstract—Borna disease virus (BDV) is a neurotropic, non-cytolytic RNA virus which replicates in the cell nucleus targeting mainly hippocampal neurons, but also astroglial and oligodendroglial cells in the brain. BDV is associated with a large spectrum of neuropsychiatric pathologies in animals. Its relationship to human neuropsychiatric illness still remains controversial. We could recently demonstrate that human BDV strain Hu-H1 promoted apoptosis and inhibited cell proliferation in a human oligodendroglial cell line (OL cells) whereas laboratory BDV strain V acted contrariwise. Here, differential protein expression between BDV Hu-H1-infected OL cells and non-infected OL cells was assessed through a proteomics approach, using two-dimensional electrophoresis followed by matrix-assisted laser desorption ionization-time of flight tandem mass spectrometry. A total of 63 differential host proteins were identified in BDV Hu-H1-infected OL cells compared to non-infected OL cells. We found that most changes referred to alterations related to the pentose phosphate pathway, glyoxylate and dicarboxylate metabolism, the tricarboxylic acid (TCA) cycle, and glycolysis /gluconeogenesis. By manual querying, two differential proteins were found to be associated with mitogen-activated protein kinase (MAPK) signal transduction. Five key signaling proteins of this pathway (i.e., p-Raf, p-MEK, p-ERK1/2, p-RSK, and p-MSK) were selected for Western blotting validation. p-ERK1/2 and p-RSK were found to be significantly up-regulated, and p-MSK was found to be significantly down-regulated in BDV Hu-H1-infected OL cells compared to non-infected OL cell. Although BDV Hu-H1 constitutively activated the ERK–RSK pathway, host cell proliferation and nuclear translocation of activated pERK in BDV Hu-H1-infected OL cells were impaired. These findings indicate that BDV Hu-H1 infection of human oligodendroglial cells significantly perturbs host energy metabolism, activates the downstream ERK–RSK complex of the Raf/MEK/ERK signaling cascade, and disturbs host cell proliferation possibly through impaired nuclear translocation of pERK, a finding which warrants further research.

Key words: Borna disease virus, BDV, oligodendroglial cell, proteomic, energy, ERK signaling.

INTRODUCTION

Borna disease virus (BDV), a member of the family Bornaviridae in the order Mononegavirales, is an

*Correspondence to: P. Xie, Department of Neurology, The First Affiliated Hospital, Chongqing Medical University, No. 1 Yixue Road, Yuzhong District, Chongqing 400016, China. Tel: +86-23-68485490; fax: +86-23-68485111.

E-mail address: xiepeng@cqmu.edu.cn (P. Xie).

† These authors contributed equally to this work.

Abbreviations: 2-DE, two-dimensional electrophoresis; BDV C6BV, laboratory Borna disease virus strain C6BV; BDV He/80, laboratory Borna disease virus strain He/80; BDV Hu-H1, human Borna disease virus strain Hu-H1; BDV strain V, laboratory Borna disease virus strain V; BDV, Borna disease virus; CCK-8, Cell Counting Kit-8; CHAPS, 3-[(3-cholamido-propyl)-dimethylammonio]-1-propanesulfonate; CI%, protein score confidence index,; CREB, cAMP-response element-binding protein; CrkL, Crk-like protein; DAVID, Database for Annotation, Visualization, and Integrated Discovery; DMEM, Dulbecco's modified Eagle's medium; DTT, dithiothreitol; EBV, Epstein-Barr virus; ECL, enhanced chemiluminescence; ERK, extracellular-regulated kinase; FBS, fetal bovine serum; GAPDH, Glyceraldehyde-3-phosphate dehydrogenase; HBV, hepatitis B virus; HCMV, human cytomegalovirus; HCV, hepatitis C virus; HIV-1, human immunodeficiency virus; IEF, isoelectric focusing; IgG, immunoglobulin G; KEGG, Kyoto Encyclopedia of Genes and Genomes; MALDI-TOF-MS/MS, matrix-assisted laser desorption ionization-time of flight-tandem mass spectrometry; MAPK, mitogen-activated protein kinase; MEK, extracellular signal-regulated protein kinases; MOI, multiplicity of infection; MS, mass spectrometry; MSK, mitogen- and stress-activated protein kinase; NNS, non-segmented, negative-strand; NT-3, neurotrophin-3; OD, optical density; OL cells, oligodendroglial cell line; p24, Borna disease virus phosphoprotein 24; p40, Borna disease virus nuclear protein 40; PBS, phosphate-buffered saline; PEBP-1, phosphatidylethanolamine-binding protein 1; PRPP, 5-phosphoribosyl-1-pyrophosphate; PVDF, polyvinylidene fluoride; PVY, potato virus Y; Raf, rapidly accelerated fibrosarcoma; RKIP, Raf kinase inhibitor protein; RSK, 90-kDa ribosomal S6 kinase; SARS-CoV, severe acute respiratory syndrome coronavirus; SDS–PAGE, sodium dodecyl sulfate polyacrylamide gel electrophoresis; SPSS, Statistical Package of Social Science; TCA, tricarboxylic acid; TFA, trifluoroacetic acid.

http://dx.doi.org/10.1016/j.neuroscience.2014.03.009
0306-4522/

enveloped virus with a non-segmented, negative-strand (NNS) ribonucleic acid (RNA) genome (Ludwig et al., 1988; de la Torre, 1994; Schneemann et al., 1995). BDV infects a wide variety of mammal species (Ludwig and Bode, 2000; Hornig et al., 2003). Infected animal hosts develop a large spectrum of neuropsychiatric pathologies ranging from immune-mediated neurological disease to non-inflammatory behavioral alterations (Ludwig and Bode, 2000), which are notably reminiscent of symptoms observed in certain human neuropsychiatric disorders (Hornig et al., 2001). Therefore, several studies have attempted to conclusively associate BDV with human psychiatric illness, but the findings remain controversial (Bode et al., 1995; Iwata et al., 1998; Kim et al., 1999; Fukuda et al., 2001; Ikuta et al., 2002; Bode and Ludwig, 2003; Hornig et al., 2012). Regardless of this debate, a few human BDV strains could have been finally recovered in Germany, through laborious, long-term co-cultivation of freshly isolated white blood cells from psychiatric inpatients with a human oligodendroglial cell line (OL cells) (Bode et al., 1996). Genetic analyses could validate both the identity of BDV RNA in the original samples and the corresponding isolates, and their authenticity as human viruses, as they differ genetically from the laboratory reference BDV strain V and another lab strain termed C6BV by few but distinct and meaningful mutations in each gene (de la Torre et al., 1996). Moreover, our previous metabonomic research has demonstrated that one of these human strains, BDV Hu-H1, which had been isolated from a severely depressed, hospitalized bipolar patient's PBMCs, perturbs energy metabolites in OL cells (Huang et al., 2012). Even more interesting, our group could have found last year that BDV Hu-H1 differed remarkably from the laboratory-adapted BDV strain V. In fact, BDV Hu-H1 inhibited proliferation and promoted apoptosis in OL cells, while strain V displayed the opposite effects (Li et al., 2013). Lab strain V was originally isolated from a diseased horse in Germany in the late 1920s, underwent numerous *in vivo* passages in rabbits and rats followed by multiple cell culture passaging.

OL cells are a cell line derived from fetal human oligodendrocytes and passaged at least 100 times. Oligodendrocytes are a major cellular component of the brain white matter that plays a pivotal role in maintaining neurological function via producing myelin proteins. Another human oligodendroglial cell line (HOG) derived from surgically removed oligodendrocytes was recent shown to be able to develop myelin-like sheaths (Bello-Morales et al., 2011). OL cells had successfully served as target cells for several neurotropic NNS RNA viruses, e.g. canine distemper virus (Muller et al., 1995), measles virus (Baczko et al., 1988), and BDV (Ibrahim et al., 2002; Qian et al., 2010). Although neurons are the major targets of BDV, the cell spectrum in the brain includes astroglia and oligodendroglia, as well (Carbone et al., 1993). Various cell types and viral strains have been shown to differentially affect BDV's influence on the host (Williams et al., 2008; Poenisch et al., 2009; Wu et al., 2013), including our above-mentioned study (Li et al., 2013). However, a better insight into the mechanism, how BDV and the human strain in particular the human BDV strain manipulates its host cells *in vitro*, should support our understanding of BDV's neuropathogenesis *in vivo*.

Up to now, mass spectrometry (MS)-based proteomics have been successfully applied to study the effects of viral infections on the host cell proteome (Zheng et al., 2011). For instance, proteomic profiling methods have revealed considerable pathophysiological changes in neurons infected with BDV laboratory strain He/80 (BDV He/80) (Suberbielle et al., 2008). However, no proteomic study has yet assessed a wild-type BDV strain, like the human virus BDV Hu-H1 and how infection impacts on the differential protein expression of host cells, like the human oligodendroglial cell line (OL cells). Therefore, in this study, we comparatively analyzed BDV Hu-H1- and non-infected OL cells by two-dimensional electrophoresis (2-DE) followed by matrix-assisted laser desorption ionization-time of flight-tandem mass spectrometry (MALDI-TOF-MS/MS) and further bioinformatics- and biochemistry-based methods. The study is focused on the identification of energy metabolites and mitogen-activated protein kinase signaling proteins.

EXPERIMENTAL PROCEDURES

Cell lines and viral strain

The human oligodendroglial cell line termed OL cells, originally derived from fetal human oligodendrocytes, (112 passages), and the human BDV Hu-H1 strain (77 passages in OL cells) (Bode et al., 1996) were kindly supplied by Hanns Ludwig (Free University of Berlin, Berlin, Germany). Persistently-infected OL cells and non-infected OL cells were cultured in Dulbecco's modified Eagle's medium (DMEM; Hyclone, Logan, Utah, USA) with 10% fetal bovine serum (FBS, Hyclone), 100 U/ml penicillin, and 100 μg/ml streptomycin (Hyclone) within a humidified incubator (5% CO_2, 37 °C) and were passaged when they reached 90% confluence by trypsinization (Hyclone).

Viral solution preparation, titration, and infection

OL cells were sub-cultured in one 10-cm dish and infected with BDV Hu-H1 stock solution at a multiplicity of infection (MOI) of 1.0 as described previously (Huang et al., 2012). Specifically, cells were washed twice with serum-free DMEM before 800 μl of stock viral solution was added to the dish. Cells were then stored in a humidified incubator (5% CO_2, 37 °C) for two hours with gentle shaking for 15 min. Excess virus was removed by washing with 5 ml of serum-free DMEM before bathing the cells in 10 ml of culture medium (10% FBS in DMEM). To achieve persistent infection and stable viral titration, the Hu-H1-infected OL cells (112 OL passages, 0 Hu-H1 passages) were cultured and passaged until all cells were infected with BDV Hu-H1 (142 OL passages, 30 Hu-H1 passages). An immunofluorescence assay was applied to stain BDV-specific nucleoprotein p40 in

order to monitor the state of the OL cells. The now persistently-infected (OL/Hu-H1 cells) and non-infected OL cells (control cells) were kept under identical conditions for the remainder of the study.

Protein extract and 2-DE sample preparation

After cell scraping and three washes with phosphate-buffered saline (PBS, pH 7.4, 0.01 M), cells were centrifuged at 500*g* for 5 min at 4 °C. Separate pooled samples of OL/Hu-H1 cells and control cells were generated by combining equal volumes of the six 10-cm dishes from each group of cells. Proteins were dissolved in a dissociation solution (7 mM urea, 2 M thiourea, 4% 3-[(3-cholamido-propyl)-dimethylammonio]-1-propanesulfonate (CHAPS), 50 mM dithiothreitol (DTT), 0.2% 3–10 Bio-Lyte; Bio-Rad Laboratories, Hercules, CA, USA), and the concentration of protein dilutions content was determined by the Bradford assay. Immediately prior to isoelectric focusing (IEF), each sample was further diluted to 100 μg/350 μl with dissociation solution.

Two-dimensional electrophoresis (2-DE)

Each sample was run in triplicate to control for gel variation; therefore, six analytical gels (three Hu-H1 gels and three control gels) with 100-μg loading were developed. In the first-dimension IEF phase, 17-cm IPG strips (pH 3–10 NL; Bio-Rad) were used. After passive rehydration for a minimum of 12 h, the strips were focused and stained as previously described (Yang et al., 2013). The six analytical gels were scanned using an Epson 10000XL scanner (Epson Co., Ltd., Beijing, China) at an optical resolution of 300 dpi. Image analysis and spot detection were accomplished with PDQuest software version 8.0.1 (Bio-Rad) using Gaussian spot modeling. For quantitative comparison of spots across gels, replicate images of the gels were created. To correct for the variability in silver staining, the individual spot volumes were normalized by dividing each spot's optical density (OD) value by the sum total OD of all spots in the respective gel. This method controlled for differences in sample loading and color intensities among the gels. Automated and manual spot matching were also performed. Only integrated intensities demonstrating at least a 1.5-fold change were applied to determine the statistical differences in protein expression between the two groups (Yang et al., 2013).

Protein identification by MALDI-TOF-MS/MS

The protein spots of interest were excised from the preparative gels with 250-μg loading and destained. After reduction and alkylation, the gel slices were digested overnight with sequencing grade-modified trypsin (Promega, Madison, WI, USA). The digested peptides were extracted with 100 μl 60% acetonitrile (Merck, Darmstadt, Germany) containing 0.1% trifluoroacetic acid (TFA) (Merck) and concentrated in a Speed Vac (Savant Instruments, Inc., Hicksville, NY, USA). The peptides were redissolved using a matrix solution, spotted on a MALDI target plate, and analyzed using the 4800 Plus MALDI TOF/TOF Analyzer (Applied Biosystems, Foster City, CA, USA) in the default mode. The MS spectra were recorded in reflector mode in a mass range from m/z 800 to 4000 with a focus mass of m/z 2000. MS used a CalMix5 standard to calibrate the instrument (ABI 4800 Calibration Mixture). For each MS spectrum, 25 subspectra with 125 shots per subspectrum were accumulated using a random search pattern. For MS calibration, autolysis peaks of trypsin ([M + H] + 842.5100 and 2211.1046) were used as internal calibrates, and up to 10 of the most intense ion signals were selected as precursors for MS/MS acquisition (excluding the trypsin autolysis peaks and the matrix ion signals). In MS/MS-positive ion mode, 50 subspectra with 50 shots per subspectrum were accumulated using a random search pattern for each MS spectrum.

The data search was conducted on GPS Explorer (Version 3.6, AB SCIEX, Foster City, CA, USA) using the search engine Mascot (Version 2.2, Matrix Science, London, UK) against the following NCBI *Homo sapiens* database (248,112 sequences) and NCBI bornavirus database (372 sequences). Search parameters were set as follows: enzyme = trypsin, allowance = up to one missed cleavage, peptide mass tolerance = 100 ppm, fragment mass tolerance = 0.4 Da, fixed modification = carbamidomethylation (Cys), and variable modification = oxidation (Met). A protein score confidence index (CI%) of 95% was used for further manual validation (Yang et al., 2013).

Bioinformatic analysis

In order to identify the enriched pathways, the protein data identified from MALDI-TOF-MS/MS were entered into DAVID Bioinformatics Resources v6.7 (http://david.abcc.ncifcrf.gov/home.jsp) (Dennis et al., 2003) to obtain the Kyoto Encyclopedia of Genes and Genomes (KEGG) terms (www.genome.jp/kegg/). The KEGG pathways with a corrected *P*-value of less than 0.05 were deemed to be statistically significant.

Western blotting

To validate the effects of BDV Hu-H1 infection on phosphatidylethanolamine-binding protein 1 (PEBP-1), Crk-like protein (CrkL) and the Raf/MEK/ERK signaling cascade (i.e., p-Raf, p-MEK, p-ERK1/2, p-RSK, and p-MSK), the seven proteins were selected for Western blotting analysis. Beta-tubulin or Glyceraldehyde-3-phosphate dehydrogenase (GAPDH) was used as a loading control (both diluted 1:30,000). Monolayers of OL/Hu-H1 and control cells were lysed in the standard lysis buffer, sonicated on ice, and 10-μg lysates were separated by 10% sodium dodecyl sulfate–polyacrylamide gel electrophoresis (SDS–PAGE) and transferred onto a polyvinylidene fluoride (PVDF) membrane. The membranes were incubated overnight at 4 °C with anti-PEBP-1, and anti-CrkL rabbit antibodies (both diluted 1:1000; Abcam, Cambridge, MA, USA) in addition to anti-

p-Raf, anti-p-MEK, anti-p-ERK, anti-p-RSK, anti-p-MSK rabbit antibodies (all diluted 1:500; CST, Beverly, MA, USA), respectively. All membranes were washed and incubated with horseradish peroxidase-coupled anti-rabbit immunoglobulin G (IgG) (diluted 1:5000, Bio-Rad; diluted 1:2000, CST). After extensive washing, antibody-detected protein bands were visualized by enhanced chemiluminescence (ECL) and exposed to autoradiography film.

Assays for cell proliferation with and without ERK inhibitor U0126

OL/Hu-H1 cells and OL cells were plated into 96-well plates at 2.5×10^4 cells per well in DMEM/F12 medium containing 10% fetal calf serum (FCS), respectively. The cells were allowed to grow to 80% confluency and switched to serum-free medium in the absence or presence of ERK inhibitor U0126 (40 μM, CST). After 24 h, they were harvested and assayed using Cell Counting Kit-8 (CCK-8) (Beyotime, Jiangshu, China).The mean absorption of four independent assays was plotted with SD for each group.

Immunofluorescence and co-localization analysis

Both OL/Hu-H1 cells and control OL cells were grown on six-well dishes for 30 min at room temperature with 4% paraformaldehyde followed by permeabilization for 5 min in 0.4% Triton X-100. Thereafter, both lines were rinsed with PBS and blocked with 5% (w/v) skimmed milk solution for one hour at 37 °C. Overnight incubation with anti-pERK antigen primary monoclonal antibody (diluted 1:200; CST, Beverly, MA, USA) at 4 °C was followed by one hour of incubation with TRITC-labeled anti-rabbit IgG (diluted 1:200, Santa Cruz Biotechnology, Santa Cruz, USA) at room temperature. After three PBS washes, immunofluorescence was detected by phase-contrast microscopy. We studied the co-localization of pERK in the nucleus using ImageJ software with the Intensity Correlation Analysis plugin (Li et al., 2004).

Statistical analysis

Statistical analysis was performed using the Statistical Package of Social Science (SPSS) for Windows version 19.0. The Wilcoxon test was used to analyze significant differences between the two cell groups. All tests were two-tailed, and the significance level was set at $p < 0.05$.

RESULTS

Experimental setup

To analyze the impact of BDV Hu-H1 persistence on the proteome of human OL cells, we applied a 2-DE-MALDI-TOF-MS/MS approach to cellular extracts prepared from OL cells infected or not infected with BDV Hu-H1 which were subsequently digested with trypsin. The whole experimental process is schematically shown in a work flow diagram (Fig. 1).

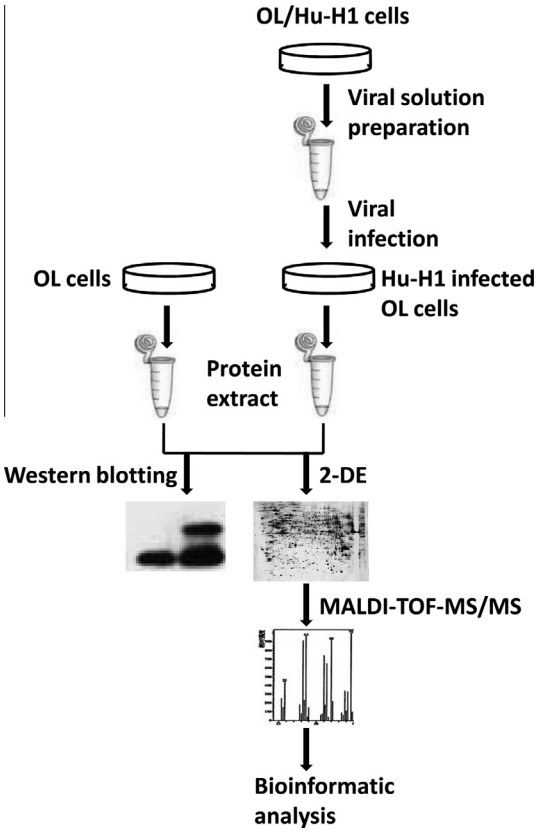

Fig. 1. Work flow diagram. Whole-cell extracts were prepared from BDV Hu-H1-infected and non-infected control OL cells. A 2-DE-MALDI-TOF-MS/MS approach was used to comparatively analyze the two groups. Further biochemistry was applied to validate the MS analysis results.

Differential protein spotting from 2-DE

Approximately 1900 protein spots on the 3–10 NL range gels were identified by silver staining (Fig. 2). Through differential analysis of the 3–10 NL pH range gels with PDQuest software, 86 differential spots were identified in OL/Hu-H1 cells compared to control cells of which 35 spots up-regulated and 51 spots down-regulated.

MALDI-TOF-MS/MS identification of differential proteins

Of the 86 spots originally detected using PDQuest analysis, several spots could not be obtained from the subsequent preparative gels after increasing the loading amount from 100 to 250 μg. As a result, only 76 protein spots (72 host protein spots and four BDV protein spots) were excised from the preparative gels for MALDI-TOF MS/MS analysis. Finally, 63 non-redundant differential host proteins originating from the 72 host protein spots, and three differential BDV proteins of the originally four BDV protein spots were successfully identified (Table 1), yielding a MS identification ratio of 90.7%.

Altered pathways by bioinformatic analysis

63 differential host proteins were analyzed for KEGG over-representation of pathways (“proteomic phenotyping”) to

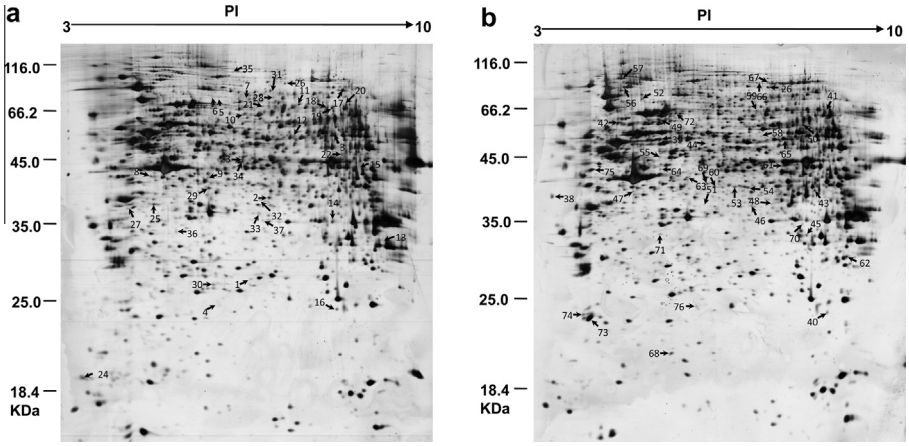

Fig. 2. Differential protein spotting by two-dimensional electrophoresis (2-DE). 2-DE gel images of (a) control cells and (b) OL/Hu-H1 cells. Approximately 1900 protein spots on gels with the 3–10 NL range were identified by silver staining. A total of 72 differential host protein spots (spots 1–72, numbered with arrows) representing 63 unique differential host proteins were identified. Additionally, four differential spots (spots 73–76, numbered with arrows) representing three unique BDV proteins were identified.

obtain functional insights into the differences between Hu-H1 and control cells. Only 26 of the 63 differential host cell proteins were mapped onto the KEGG database. The resulting top ten-ranking canonical KEGG pathways are listed in Table 2. Energy metabolism was the most statistically over-represented set of pathways with pentose phosphate pathway ranking first ($p < 0.001$), glyoxylate and dicarboxylate metabolism ranking second ($p < 0.01$), tricarboxylic acid (TCA) cycle ranking fourth ($p < 0.05$), and glycolysis/gluconeogenesis ranking eighth ($p < 0.05$). Moreover and through manual querying, two proteins associated with the Raf/MEK/ERK signaling cascade, PEBP-1 and CrkL, were found to be dysregulated in OL/Hu-H1 cells compared to control cells.

Detection of differential proteins and the Raf/MEK/ERK signaling cascade by Western blotting

Based on the aforementioned analysis, two differential proteins – PEBP-1 and CrkL (Fig. 3), five key Raf/MEK/ERK signaling proteins – p-Raf, p-MEK, p-ERK1/2, p-RSK, and p-MSK, were selected for validation by Western blotting (Fig. 4). PEBP-1 ($p = 0.015$), p-ERK1/2 ($p = 0.016$) and p-RSK ($p = 0.0495$) were found to be significantly up-regulated, CrkL ($p = 0.03$) and p-MSK ($p = 0.024$) was found to be significantly down-regulated, in OL/Hu-H1 cells compared to control cells. There was no significant dysregulation observed in p-Raf ($p = 0.744$) or p-MEK ($p = 0.267$).

BDV Hu-H1 decreases OL cell proliferation

Based on the finding of up-regulated pERK in response to BDV Hu-H1 infection, CCK-8 assay was performed on cells treated with or without ERK inhibitor U0126 in OL/Hu-H1and control cells. The data, seen in Fig. 5, clearly demonstrated that BDV Hu-H1 infection decreased OL cell proliferation ($p < 0.05$). ERK inhibitor U0126 decreased OL cell proliferation ($p < 0.05$) but did not significantly decrease the impaired OL/Hu-H1 cell proliferation any further ($p > 0.05$).

Impaired nuclear translocation of pERKs

Anti-pERK antibody labeling and subsequent immunofluorescence analysis were carried out in OL/Hu-H1 cells and control OL cells. Co-localization of pERK and nucleus was studied using ImageJ software with the Intensity Correlation Analysis plugin. As shown in Fig. 6a, BDV Hu-H1 induced lower presence of pERK in the nucleus and higher presence in the cytoplasm than control OL cells. As shown in Fig. 6b, analyzed by using ImageJ software with the Intensity Correlation Analysis plugin, the co-localization of pERK and nucleus in OL/Hu-H1 cells was significantly lower than in control cells ($p = 0.04$), suggesting impaired nuclear translocation of pERK in response to BDV Hu-H1 infection.

DISCUSSION

In this study, a 2-DE-MALDI-TOF-MS/MS approach was used to comparatively analyze BDV Hu-H1-infected and non-infected control OL cells. Several previous studies have also applied 2-DE/MS-based proteomic approaches to identify and analyze differential host proteins across a range of viral infections (e.g., BDV, Epstein-Barr virus (EBV), hepatitis B virus (HBV), hepatitis C virus (HCV), human immunodeficiency virus (HIV-1), and severe acute respiratory syndrome coronavirus (SARS-CoV)) (Zhou et al., 2011). With respect to BDV, the study by Suberbielle et al. had focused on BDV-induced effects on the complex neuronal proteome. They found significant protein changes, among others referring to synaptic activity. They compared the proteomes of laboratory strain BDV He/80-infected and non-infected primary cultured embryonic Sprague–Dawley rat cortical neurons, using two-dimensional liquid chromatography fractionation, followed by protein identification through nanoliquid

Table 1. Differential proteins identified by MALDI-TOF/TOF MS

Spot No.	GI No.	Gene name	Protein name	Mascot score	Protein Score C. I.%	MW (Da)	PI	Biological function	Fold-change (Hu-H1/CON)
Host Proteins (63)									
1	116875831	RMDN1	Regulator of microtubule dynamics protein 1 [*Homo sapiens*]	473	100	36,013.4	8.64	Microtubule-associated protein	−1.92
2	119599451	MRPS22	Mitochondrial ribosomal protein S22, isoform CRA_e [*Homo sapiens*]	645	100	36,839.9	6.34	Translation of mitochondrial mRNAs	−1.96
3	12652799	C22orf28	Chromosome 22 open reading frame 28 [*Homo sapiens*]	238	100	55,722	6.77	tRNA-splicing ligase complex	−3.23
4	14249382	ABHD14B	Abhydrolase domain-containing protein 14B isoform 1[*Homo sapiens*]	281	100	22,445.6	5.94	Transcription activation	1.54
5	14495609	CTPS1	CTP synthase [*Homo sapiens*]	81	99.807	67,358.3	6.02	Pyrimidine metabolism	4.17
6				81	99.807	67,358.3	6.02		4.17
7	194383562		cDNA FLJ58563, highly similar to CTP synthase 1 (EC 6.3.4.2)	160	100	50,233.4	7.23		−1.56
8	15277503	ACTB	ACTB protein, partial [*Homo sapiens*] (Beta-actin)	525	100	40,536.2	5.55	Cell motility	3.45
9				461	100	40,536.2	5.55		3.45
10	157426879	NPLOC4	Nuclear protein localization protein 4 homolog [*Homo sapiens*]	241	100	69,046.2	5.94	NPLOC4-UFD1L-VCP complex	−3.57
11	158261431	NSF	Vesicle-fusing ATPase	452	100	83,059.2	6.38	Synaptic vesicle cycle	−2.22
12	1688076	DNAJC7	Tetratricopeptide repeat protein [*Homo sapiens*]	629	100	56,185.6	7.08	Steroid receptors folding	−5.26
13	18645167	ANXA2	Annexin A2 [*Homo sapiens*]	851	100	38,779.9	7.57	Heat-stress response,	−12.5
14				1100	100	40,730.9	8.41	membrane-binding	1.68
15	189054178	KRT1	Keratin, type II cytoskeletal 1	141	100	66,151	7.62	Keratinization	−1.96
16	193783553	SOD2	Superoxide dismutase	171	100	19,832	7.81	Peroxisome	−2.78
17	194380306	ACO2	cDNA FLJ51705, highly similar to aconitate hydratase, mitochondrial (EC 4.2.1.3)	797	100	84,102.3	7.62	Glyoxylate and dicarboxylate metabolism, TCA cycle	−3.03
18	194382840	FUBP1	cDNA FLJ61021, highly similar to Far upstream element-	595	100	66,361.9	7.12	RNA binding	1.5
19			binding protein 1 (FBP1)	777	100	66,361.9	7.12		1.5
20				802	100	66,361.9	7.12		1.5
21	14603253	PGM2	Phosphoglucomutase 2 [*Homo sapiens*]	206	100	68,811.6	6.17	Pentose phosphate pathway, glycolysis/gluconeogenesis	2.6
22	194385880	NLE1	cDNA FLJ57449, highly similar to Notchless homolog 1	78	99.65	48,962.8	6.14	Notch signaling pathway	−1.75
23	194390424	EEF1G	Elongation factor 1-gamma, cDNA FLJ56389, highly similar to Elongation factor 1-gamma	471	100	56,456.5	7.6	Translation elongation factor activity	−1.75
24	9910382	TOMM22	Mitochondrial import receptor subunit TOM22 homolog [*Homo sapiens*]	401	100	15,511.8	4.27	Protein transport	−1.54
25	210032390	SEC13	Protein SEC13 homolog isoform 2 [*Homo sapiens*]	576	100	34,503.6	5.4	RNA transport	1.61
26	8659555	ACO1	Cytoplasmic aconitate hydratase [*Homo sapiens*]	682	100	98,849.8	6.23	Glyoxylate and dicarboxylate metabolism, TCA cycle	2.14
27	25453472	EEF1D	Elongation factor 1-delta isoform 2 [*Homo sapiens*]	696	100	31,216.8	4.9	Regulation of heat-shock-responsive genes induction	3.25
28	28436809	RDX	Radixin [*Homo sapiens*]	493	100	68,636.4	5.88	Regulation of actin cytoskeleton	1.64
29	30704877	C12orf10	Chromosome 12 open reading frame 10 [*Homo sapiens*]	179	100	42,823.6	6.35	Unknown	−1.59
30	32483377	PRDX3	Thioredoxin-dependent peroxide reductase,mitochondrial isoform b [*Homo sapiens*] (AOP-1)	496	100	26,107.4	7.04	Redox regulation	2.86
31	33469968	MCM7	DNA replication licensing factor MCM7 isoform 1 [*Homo sapiens*]	994	100	81,883.8	6.08	DNA replication	1.53

(*continued on next page*)

Table 1 (*continued*)

Spot No.	GI No.	Gene name	Protein name	Mascot score	Protein Score C. I.%	MW (Da)	PI	Biological function	Fold-change (Hu-H1/CON)
32	33589854	BLVRA	Biliverdin reductase A precursor [*Homo sapiens*]	293	100	33,692.4	6.06	Porphyrin and chlorophyll metabolism	1.54
33	350276247	PPP1CC	Serine/threonine-protein phosphatase PP1-gamma catalytic subunit isoform 2 [*Homo sapiens*]	708	100	39,234.7	5.8	Regulation of actin cytoskeleton	−2.17
34	386781221	WDR4	tRNA (guanine-N(7)-)-methyltransferase subunit WDR4 isoform 2 [*Homo sapiens*]	350	100	46,074.2	6.47	tRNA modification, RNA (guanine-N7)-methylation	3.66
35	40788339	MATR3	KIAA0723 protein [*Homo sapiens*] (Matrin-3)	317	100	95,681.3	5.91	Transcription regulation	2.79
36	40788883	MLEC	KIAA0152 [*Homo sapiens*] (Malectin)	492	100	34,385.8	5.6	Carbohydrate metabolism	−2.27
37	4502101	ANXA1	Annexin A1 [*Homo sapiens*]	635	100	38,918.1	6.57	Membrane fusion	1.56
38	4502891	CLNS1A	Methylosome subunit pICln [*Homo sapiens*]	182	100	26,370	3.97	RNA transport	236.7
39	4503729	FKBP4	Peptidyl-prolyl cis–trans isomerase FKBP4 [*Homo sapiens*]	781	100	52,057.2	5.35	Estrogen signaling pathway	2.33
40	4505621	PEBP-1	Phosphatidylethanolamine-binding protein 1preproprotein [*Homo sapiens*]	390	100	21,157.7	7.01	MAPK signaling pathway	3.12
41	4507521	TKT	Transketolase isoform 1 [*Homo sapiens*]	554	100	68,519	7.58	Pentose phosphate pathway	2.14
42	460789	HNRNPK	Transformation upregulated nuclear protein [*Homo sapiens*]	106	100	51,325.5	5.13	Spliceosome	7.79
43	4758768	NDUFA10	NADH dehydrogenase [ubiquinone] 1 alpha subcomplex subunit 10, mitochondrial precursor [*Homo sapiens*]	99	99.997	41,067.1	8.67	Oxidative phosphorylation	2.85
44	48145673	HNRNPH1	HNRPH1 [*Homo sapiens*]	347	100	49,384.4	5.79	RNA Processing	−1.72
45	48146045	VDAC2	VDAC2 [*Homo sapiens*]	157	100	30,849.2	6.81	Calcium signaling pathway	3.58
46	4885153	CRKL	Crk-like protein [*Homo sapiens*]	365	100	33,870	6.26	Regulation of actin cytoskeleton, MAPK signaling pathway	−1.56
47	4885585	SAE1	SUMO-activating enzyme subunit 1 isoform a [*Homo sapiens*]	524	100	38,881.7	5.17	Ubiquitin-mediated proteolysis	1.82
48	49456481	TWF1	PTK9 [*Homo sapiens*] (Twinfilin-1)	511	100	40,476.8	6.65	Cytoskeleton regulation	−2.00
49	5031703	G3BP1	Ras GTPase-activating protein-binding protein 1 [*Homo sapiens*]	321	100	52,189.1	5.36	Nucleic acid metabolic process	1.67
50	5031875	LMNA	Lamin isoform C [*Homo sapiens*]	656	100	65,152.6	6.4	Cellular structural protein, cell senescence	−2.86
51	54696354	PPP1CB	Protein phosphatase 1, catalytic subunit, beta isoform[*Homo sapiens*]	559	100	37,944.9	5.84	Regulation of actin cytoskeleton	13.71
52	556514	APEH	Acylamino acid-releasing enzyme [*Homo sapiens*] (AARE)	639	100	82,210	5.29	Serine-type endopeptidase activity	1.94
53	55956921	HNRNPAB	Heterogeneous nuclear ribonucleoprotein A/B isoform b	126	100	30,683.1	7.68	RNA Binding	−1.92
54			[*Homo sapiens*]	285	100	30,683.1	7.68		−1.92
55	5730023	RUVBL2	RuvB-like 2 [*Homo sapiens*]	314	100	51,295.6	5.49	NuA4 histone acetyltransferase complex	2.03
56	6005942	VCP	Transitional endoplasmic reticulum ATPase [*Homo sapiens*]	602	100	89,950	5.14	DNA damage and repair	2.2
57	62087882	HSPA4	Heat shock 70 kDa protein 4 isoform a variant [*Homo sapiens*]	866	100	88,804.5	5.44	Stress response	−2.5
58	119628379	CCT6A	Chaperonin containing TCP1, subunit 6A (zeta 1),isoform CRA_b [*Homo sapiens*]	70	97.216	39,433.9	6.74	Protein folding	−2.08
59	62089196	TRAP1	TNF receptor-associated protein 1 variant [*Homo sapiens*]	605	100	80,227.8	8.32	Stress response	−1.54
60	62896593	ENO1	Enolase 1 variant [*Homo sapiens*]	112	100	47,453.4	7.01	Glycolysis/gluconeogenesis	−2
61				109	100	47,509.4	7.01		−2.94
62	62897701	SNRPA1	Small nuclear ribonucleoprotein polypeptide A' variant [*Homo sapiens*]	150	100	28,498.2	8.72	Spliceosome	12.44

63	62897067	TARDBP	TAR DNA binding protein variant [*Homo sapiens*]	325	100	44,981.4	6.03	Transcription and splicing	12.16
64	6330926	GDA	KIAA1258 protein [*Homo sapiens*]	228	100	53,915	5.51	Guanine catabolic process	3.48
65	66933016	IMPDH2	Inosine-5′-monophosphate dehydrogenase 2 [*Homo sapiens*]	1000	100	56,225.8	6.44	RNA and/or DNA metabolism	2.04
66	7020309	NSUN2	tRNA (cytosine(34)-C(5))-methyltransferase	171	100	59,884.2	6.14	RNA methylation	6.62
67				309	100	59,884.2	6.14		6.62
68	70906444	DUT	Deoxyuridine 5′-triphosphate nucleotidohydrolase,mitochondrial isoform 3 [*Homo sapiens*]	68	95.882	15,499.8	6.13	Nucleotide metabolism	−1.61
69	72534748	MRI1	Methylthioribose-1-phosphate isomerase isoform 1[*Homo sapiens*]	309	100	39,467.5	5.89	Isomerase, cell invasion	−2.22
70	189053418	PRPS1L1	Ribose-phosphate pyrophosphokinase	212	100	35,181.1	7.1	Pentose phosphate pathway	−1.96
71	73917051	PPIE	Cyclophilin-33B [*Homo sapiens*]	353	100	35,226.5	5.84	RNA splicing, protein folding	−1.52
72	763431	ALB	Albumin-like [*Homo sapiens*]	114	100	53,416.4	5.69	Colloidal osmotic pressure	3.82
BDV Proteins (3)									
73	52421808	p24	Phosphoprotein 24 (fragment) OS = Borna disease virus PE = 4 SV = 1	994	100	18,315.4	6.2	Interference with cell signaling	N/A
74	7415650			575	100	14,941.6	4.86		
75	195957122	L	Polymerase (fragment) OS = Borna disease virus GN = L PE = 4 SV = 1	40	96.365	19,917.6	9.6	Polymerase activity	N/A
76	346720747	X	X protein OS = Bornavirus goose/SP-2011/USA PE = 4 SV = 1	43	98.219	9779	9.02	Facilitates p24 export from nucleus to cytoplasm	N/A

chromatography-tandem MS (Suberbielle et al., 2008). However, to our knowledge, this is the first proteomic-based investigation which uses a wild-type BDV virus of human origin (BDV Hu-H1) to analyze its impact on a white matter-derived human oligodendroglial cell line.

Applying the foregoing approach, 63 unique differential host proteins were identified (Table 1), and bioinformatic analysis revealed that energy metabolism and mitogen-activated protein kinase (Raf/MEK/ERK) signaling cascade, which are discussed in further detail below, were significantly altered in BDV Hu-H1-infected OL cells compared to the non-infected control cells.

Energy metabolism

Through KEGG analysis, energy metabolism (i.e., pentose phosphate pathway, glyoxylate and dicarboxylate metabolism, the TCA cycle, and glycolysis/gluconeogenesis) was identified as the most significantly altered set of host biological pathways (Table 2). Viral replication requires energy and macromolecular precursors derived from the metabolic network of the host cell. Metabolic flux studies have revealed that large DNA viruses like herpes viruses are able to actively redirect energy metabolism in the host cell rather than passively relying on basal host cell metabolic activity (Vastag et al., 2011). Human cytomegalovirus (HCMV) and HSV-1 infection significantly perturb glycolysis, TCA cycle, and pentose phosphate pathway intermediates in host cells. Hepatitis C virus (HCV) has been shown to significantly upregulate host cell glycolysis (Diamond et al., 2010). Our own previous metabolic study has shown a downstream equilibrium shift away from glycolysis in conjunction with increased carbon flux through the TCA cycle in BDV-infected OL cells (Huang et al., 2012).

This study's findings expand upon previous reports by showing energy metabolic dysfunction through significant alterations in six differential proteins in OL/Hu-H1 cells compared to control cells. As summarized in Table 1, three pentose phosphate pathway proteins (ribose-phosphate pyrophosphokinase↓, transketolase 1↑, and phosphoglucomutase 2↑), one glycolytic protein (enolase 1↓), and two TCA cycle and glyoxylate and dicarboxylate metabolic proteins (cytoplasmic aconitate hydratase↑ and cDNA FLJ51705↓ [highly similar to mitochondrial aconitate hydratase]) were found to be down- or up-regulated (see arrows in text).

Ribose-phosphate pyrophosphokinase, alternatively termed 5-phosphoribosyl-1-pyrophosphate (PRPP) synthetase, catalyzes the conversion of ribose 5-phosphate into PRPP that is essential to RNA synthesis. Previous studies on HCMV and a plant virus – potato virus Y (PVY) infecting tobacco have shown ribose-phosphate pyrophosphokinase upegulation in infected cells, suggesting the enyzme's role in de novo viral nucleic acid biosynthesis via the pentose phosphate pathway (Šindelář and Šindelářová, 1987; Predmore, 2011). The here found down-regulation of ribose-phosphate pyrophosphokinase in OL/Hu-H1 cells is in constrast to these findings in DNA viruses,

Table 2. Top 10-ranking canonical KEGG pathways associated with differential proteins

KEGG pathway	Number of molecules		Fisher test *p*-value
	Mapping	All	
Pentose phosphate pathway	3	25	$3e^{-4}$
Glyoxylate and dicarboxylate metabolism	2	15	$2.5e^{-3}$
Regulation of actin cytoskeleton	5	215	$4.1e^{-3}$
Tricarboxylic acid (TCA) cycle	2	31	$1.07e^{-2}$
Focal adhesion	4	201	$1.79e^{-2}$
Spliceosome	3	126	$2.55e^{-2}$
Insulin signaling pathway	3	135	$3.05e^{-2}$
Glycolysis/gluconeogenesis	2	60	$3.71e^{-2}$
Purine metabolism	3	153	$4.19e^{-2}$
Long-term potentiation	2	68	$4.66e^{-2}$

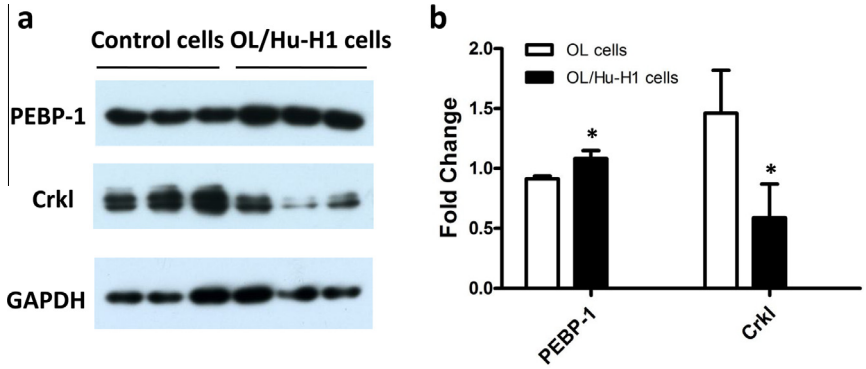

Fig. 3. Western blotting validation of PEBP-1 and Crkl. (a) Western blotting of PEBP-1 and Crkl with Glyceraldehyde-3-phosphate dehydrogenase (GAPDH) used as a control. (b) PEBP-1 ($p = 0.015$) was found to be significantly up-regulated, and Crkl ($p = 0.03$) was found to be significantly down-regulated, in OL/Hu-H1 cells compared to control cells.

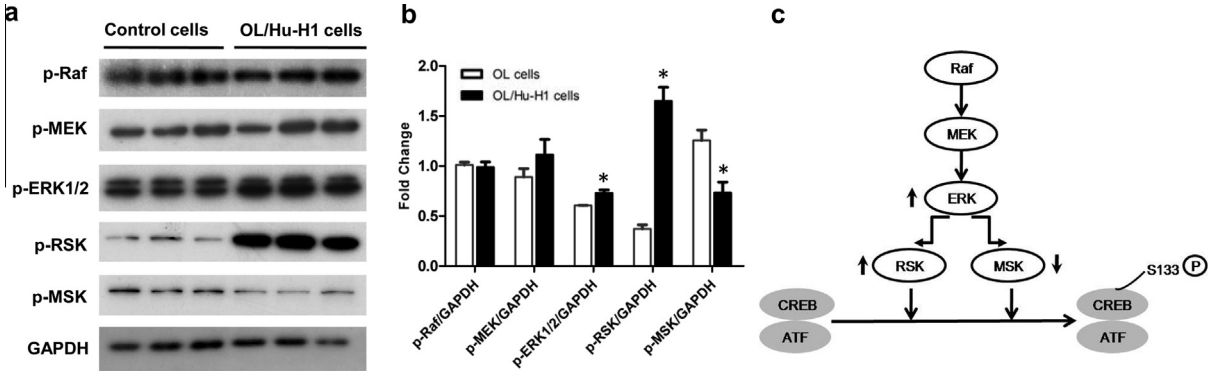

Fig. 4. Western blotting validation of Raf/MEK/ERK signaling proteins. (a) Western blots of five key Raf/MEK/ERK signaling proteins (i.e., p-Raf, p-MEK, p-ERK1/2, p-RSK, and p-MSK) with Glyceraldehyde-3-phosphate dehydrogenase (GAPDH) used as a control. (b) P-ERK1/2 ($P = 0.016$) and p-RSK ($P = 0.0495$) were found to be significantly up-regulated, and p-MSK ($P = 0.024$) was found to be significantly down-regulated, in OL/Hu-H1 cells relative to control cells. There was no significant dysregulation observed in p-Raf ($P = 0.744$) or p-MEK ($P = 0.267$). (c) Activation of the Raf/MEK/ERK signaling cascade in human OL cells induces downstream phosphorylation of the transcription factor CREB through RSK and MSK.

suggesting that BDV Hu-H1 infection favors ribose 5-phosphate over RNA's biosynthetic precursor PRPP. However, this observation is consistent with BDV's characterization as a slow-replicating virus which is able to establish persistence with a lack of demonstrable viral particles (Ludwig et al., 1988), an infection type that would not require high levels of de novo viral RNA biosynthesis.

Mammalian transketolase 1 connects the pentose phosphate pathway to glycolysis, feeding/extracting sugar phosphates into/from the primary carbohydrate metabolic pathways by reversibly catalyzing the transfer of two-carbon glycoaldehyde units from ketose-donors to aldose-acceptor sugars (e.g., sedoheptulose-7-phosphate + glyceraldehyde-3-phosphate ↔ ribose 5-phosphate + xylulose-5-phosphate). Consistent with our

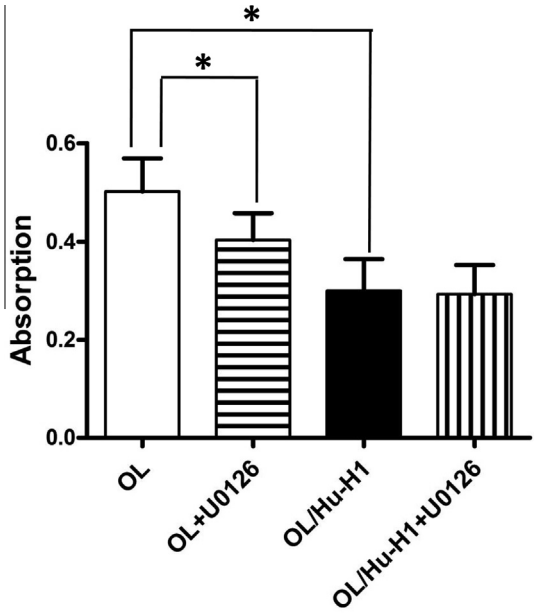

Fig. 5. Cell proliferation assay with and without ERK inhibitor U0126. Cell proliferation was detected by CCK-8 assay. Hu-H1 infection decreased OL cell proliferation. ERK inhibitor U0126 decreased OL cell proliferation but did not decrease OL/Hu-H1 cell proliferation. Data were expressed as mean ± SD of four independent experiments with similar results. $^{*}p < 0.05$ comparing to control.

current findings, transketolase (in addition to several other proteins functioning in nucleotide synthesis and homeostasis) has also been shown to be significantly up-regulated in HCV-infected human hepatocytes, supporting the metabolic rerouting into the pentose phosphate pathway that generates ribose 5-phosphate (Diamond et al., 2010).

Phosphoglucomutase 2 catalyzes the interconversion of ribose-1-phosphate and ribose-5-phosphate and also participates in glycolysis through interconverting glucose-1-phosphate and glucose-6-phosphate. Consistent with our findings in OL/Hu-H1 cells, previous studies on HCMV and H5N1 avian influenza virus have also shown phosphoglucomutase 2 upegulation in infected cells (Zou et al., 2010; Predmore, 2011). The phosphoglucomutase 2 upregulation observed in OL/Hu-H1 cells here may be associated with the aforementioned changes in ribose-phosphate pyrophosphokinase and transketolase 1, both of which affect ribose 5-phosphate levels in OL/Hu-H1 cells.

Enolase 1 is an isoenzyme of enolase, a key glycolytic enzyme that catalyzes the conversion of 2-phosphoglycerate to phosphoenolpyruvate. Previous studies on enterovirus 71 and HCV have revealed significantly up-regulated enolase 1 in rhabdomyosarcoma and heptatocellular carcinoma cell lines (Takashima et al., 2005; Leong and Chow, 2006). The here observed opposite effect of down-regulated enolase 1 in OL/Hu-H1 cells suggests a different mechanism of affecting host cell glycolysis. Interestingly, a previous metabolic analysis of HSV-1-infected cells indicates a bottleneck in glycolytic efflux at the step catalyzed by pyruvate kinase, the enzyme that converts phosphoenolpyruvate to pyruvate. This 'glycolytic bottleneck' was accompanied by increased levels of pentose phosphate pathway intermediates, thereby increasing the availability of ribose 5-phosphate (Vastag et al., 2011).Therefore, the down-regulation of enolase-1 observed in OL/Hu-H1 cells here could be an alternative 'glycolytic bottleneck'-based mechanism to increase
the availability of ribose 5-phosphate – the aforementioned upregulation of transketolase 1 and phosphoglucomutase 2 in OL/Hu-H1 cells is consistent with this conjecture.

The cytoplasmic aconitate hydratase (aconitase) and cDNA FLJ51705 (highly similar to mitochondrial aconitate hydratase) were significantly dysregulated in opposing directions. Aconitate hydratase catalyzes the isomerization of citrate to isocitrate in the TCA cycle and has a dual subcellular localization in the cytoplasm and mitochondria displaying differences in sensitivity to stimulation, inhibition, and stability (Hernanz and de la Fuente, 1988; Eprintsev et al., 2002). Therefore, one or more of these isoforms may be involved in regulatory activities independent of their traditional metabolic activities, producing the simultaneous up-regulation of one isoform and simultaneous down-regulation of another isoform observed here. Consistent with our findings, a previous proteomic study of BDV He/80-infected cortical neurons also found significant dysregulation of mitochondrial aconitate hydratase (Suberbielle et al., 2008). A comprehensive systems level study that includes transcriptomic, proteomic, and metabolic lines of analysis should clarify the precise

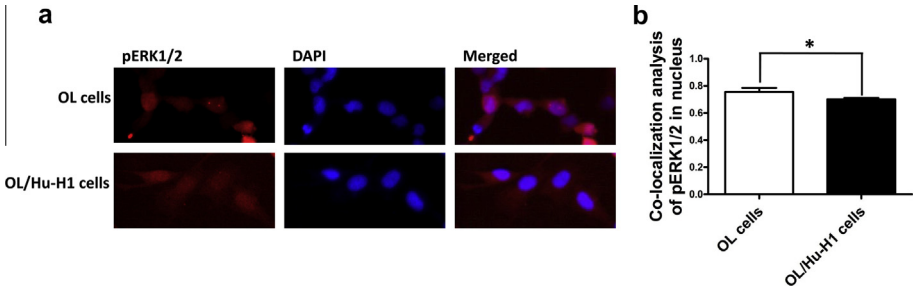

Fig. 6. Immunofluorescence and co-localization analysis of pERK1/2 in nucleus. (a) OL/Hu-H1 cells and control OL cells were analyzed for the expression of activated ERK in nucleus by immunofluorescence. (b) BDV Hu-H1 induced lower pERK in nucleus than control OL cells ($p = 0.04$), suggesting impaired nuclear translocation of pERK.

mechanism(s) by which BDV Hu-H1 impacts energy metabolism in human OL cells.

The Raf/MEK/ERK signaling cascade

Mitogen-activated protein kinase (MAPK) signal transduction cascades have been implicated in a variety of cellular functions including proliferation, differentiation, cell activation, immune responses and apoptosis (Pearson et al., 2001; Kurokawa and Kornbluth, 2009). In mammalian cells, three MAPK families have been thus far characterized: ERK, which is activated by growth factors, peptide hormones and neurotransmitters, Jun kinase (JNK) and p38 MAPK, which are both activated by cellular stress stimulus as well as growth factors (Frodin and Gammeltoft, 1999). The Raf/MEK/ERK signaling cascade is activated by many viruses, including BDV and several other human pathogenic RNA viruses (e.g., influenza, Ebola, HCV, and SARS-CoV) (Pleschka, 2008).

Here, by initial manual querying, two proteins associated with the Raf/MEK/ERK signaling cascade were found to be significantly altered in OL/Hu-H1 cells compared to control cells (arrows represent up/down-regulation in OL/Hu-H1 cells compared to control cells): PEBP-1↑ and CrkL↓. PEBP-1, alternatively termed Raf kinase inhibitor protein (RKIP), regulates Raf/MEK/ERK signaling activity by competitively disrupting the interaction between Raf and MEK, thereby negatively interfering with the downstream activation of MEK and ERK (Yeung et al., 1999). CrkL has been shown to activate the Ras/Raf signaling pathway and transform fibroblasts in a Ras-dependent fashion (Senechal et al., 1996). CrkL is down-regulated in OL/Hu-H1cells compared to control cells. Interestingly, in neurons, such down-regulation has been shown to block dendritogenesis during the development of the CA1 region in the hippocampus *in vivo* under specific conditions (Matsuki et al., 2008).

Based on these initial findings, we hypothesized that the Raf/MEK/ERK signaling cascade was perturbed in OL/Hu-H1 cells. Therefore, five key Raf/MEK/ERK signaling proteins (i.e., p-Raf, p-MEK, p-ERK1/2, p-RSK, and p-MSK) were selected for Western blotting validation (Fig. 4a). P-ERK1/2 and p-RSK were found to be significantly up-regulated, and p-MSK was found to be significantly down-regulated, in OL/Hu-H1 cells compared to control cells; however, there was no significant dysregulation observed in p-Raf or p-MEK (Fig. 4b). These combined findings indicate that BDV Hu-H1 activates the downstream ERK–RSK complex of the Raf/MEK/ERK signaling cascade in human OL cells (Fig. 4c). RSK, a substrate of ERK and a mediator of ERK signal transduction, is composed of two functional kinase domains that are activated in a sequential manner by a series of phosphorylations; MSK is a RSK-related kinase activated by ERK as well as p38 MAPK (Frodin and Gammeltoft, 1999). The activated ERK–RSK complex observed here has several proposed functions, including: (i) regulation of gene expression through phosphorylation of transcriptional regulators, such as NFκB/IκBα, cAMP-response element-binding protein (CREB), and CREB-binding protein; (ii) regulation of protein synthesis by phosphorylation of polyribosomal proteins and glycogen synthase kinase-3; and (iii) phosphorylation of the Ras GTP/GDP-exchange factor, Sos, leading to feedback inhibition of the Raf/MEK/ERK pathway (Frodin and Gammeltoft, 1999).

Many viruses manipulate the contributing kinases but differently in accord to their life cycles (Leong and Chow, 2006; Predmore, 2011; Vastag et al., 2011). Notably, BDV He/80 has also been shown to activate the Raf/MEK/ERK signaling cascade in several persistently-infected mammalian cell lines (Planz et al., 2001). In this study, BDV Hu-H1 was found to activate the ERK1/2 pathway, as well. As up-regulated pERK should increase the proliferation of cells (Seger and Krebs, 1995; Pearson et al., 2001), the CCK-8 experiment was conducted (Fig. 5) to detect proliferation and growth. In contrast to the higher ERK1/2 expression of BDV Hu-H1-infected OL cells, we found down-regulation of proliferation which was stronger than in uninfected control OL cells treated with ERK inhibitor U0126 which is apparently contradictory. However, a similar finding have been reported by Hans et al., namely that BDV activated the ERK1/2 pathway in a persistently-infected neural crest-derived cell line (PC12), but at the same time decreased the differentiation in PC cells, due to impaired translocation of ERK1/2 to the nucleus (Hans et al., 2001). We were able to show the same effects in pERK co-localization immunofluorescence assays, comparing OL/Hu-H1 cells and control OL cells (Fig. 6). Impaired translocation of key signal transduction kinases might be associated with the trafficking of viral proteins from the nucleus to the cytoplasm and vice versa, involved in nuclear replication, a unique feature of the family Bornaviridae among the order Mononegavirales (de la Torre, 1994).

Impaired translocation may at least partially explain our findings of up-regulated pERK and down-regulated proliferation in OL cells infected with a human strain of BDV. Inhibited cell proliferation was previously observed in human but not laboratory BDV (Li et al., 2013). Given the complex regulatory network between the ERK/RSK pathway, cell proliferation and programed cell death by apoptosis in multiple mammalian cell lines (for review Kurokawa and Kornbluth, 2009), the precise manner by which BDV Hu-H1's activation of the ERK–RSK complex interferes with cell proliferation and the other biological processes warrant further research.

CONCLUSION

In summary, our findings using a 2-DE-MALDI-TOF-MS/MS-based proteomic approach indicate that human BDV strain Hu-H1 manipulates brain-derived human OL cells significantly. We found 63 differential host proteins on infected vs. non-infected cells. By bioinformatic analysis, energy metabolism was the most significantly altered set of host biological pathways in BDV Hu-H1-infected OL cells. In addition, Western blotting validation demonstrated significant perturbation of the host's Raf/MEK/ERK signaling cascade: specifically, the downstream

ERK–RSK complex of the Raf/MEK/ERK signaling cascade was found to be activated by BDV Hu-H1 infection. Although BDV Hu-H1 produces constitutive activation of the ERK1/2 pathway, pERK's nuclear translocation was impaired. Further investigation on cell proliferation and other biological processes in BDV-infected oligodendrocytes and other brain cell lines is key to better understanding the neuropathogenesis of BDV.

CONFLICT OF INTEREST

The authors (Xia Liu, Yongtao Yang, Liv Bode, Mingjun Zhao, Lujun Zhang, Junxi Pan, Lin Lv, Yuan Zhan, Siwen Liu, Liang Zhang, Xiao Wang, Rongzhong Huang, Jingjing Zhou, Peng Xie) declare no conflicts of interest. Liv Bode's authorship in this study is independent of and has no relationship to her current affiliation at the Department of Epidemiology and Health Monitoring, Robert Koch Institute, Berlin, Germany.

Acknowledgments—This study was supported by the National Basic Research Program of China (973 Program) (Grant No. 2009CB918300) and the Natural Science Foundation Project of Chongqing (CSTC, 2010BB5393). We thank Wei Ding (Shanghai Applied Protein Technology Co. Ltd., Shanghai, China) for his assistance with the mass spectrometric analysis, Xiaojun Peng (Bioinformatics Center, PTM Biolab Co. Ltd, Hangzhou, Jiangsu, China) for his technical assistance with the KEGG database, Dr. N.D. Melgiri for editing and proofreading the manuscript.

REFERENCES

Baczko K, Liebert UG, Cattaneo R, Billeter MA, Roos RP, ter Meulen V (1988) Restriction of measles virus gene expression in measles inclusion body encephalitis. J Infect Dis 158:144–150.

Bello-Morales R, Perez-Hernandez M, Rejas MT, Matesanz F, Alcina A, Lopez-Guerrero JA (2011) Interaction of PLP with GFP-MAL2 in the human oligodendroglial cell line HOG. PLoS One 6:e19388.

Bode L, Durrwald R, Rantam FA, Ferszt R, Ludwig H (1996) First isolates of infectious human Borna disease virus from patients with mood disorders. Mol Psychiatry 1:200–212.

Bode L, Ludwig H (2003) Borna disease virus infection, a human mental-health risk. Clin Microbiol Rev 16:534–545.

Bode L, Zimmermann W, Ferszt R, Steinbach F, Ludwig H (1995) Borna disease virus genome transcribed and expressed in psychiatric patients. Nat Med 1:232–236.

Carbone KM, Rubin SA, Sierra-Honigmann AM, Lederman HM (1993) Characterization of a glial cell line persistently infected with borna disease virus (BDV): influence of neurotrophic factors on BDV protein and RNA expression. J Virol 67:1453–1460.

de la Torre JC (1994) Molecular biology of borna disease virus: prototype of a new group of animal viruses. J Virol 68:7669–7675.

de la Torre JC, Bode L, Durrwald R, Cubitt B, Ludwig H (1996) Sequence characterization of human Borna disease virus. Virus Res 44:33–44.

Dennis Jr G, Sherman BT, Hosack DA, Yang J, Gao W, Lane HC, Lempicki RA (2003) DAVID: Database for Annotation, Visualization, and Integrated Discovery. Genome Biol 4:P3.

Diamond DL, Syder AJ, Jacobs JM, Sorensen CM, Walters KA, Proll SC, McDermott JE, Gritsenko MA, Zhang Q, Zhao R, Metz TO, Camp 2nd DG, Waters KM, Smith RD, Rice CM, Katze MG (2010) Temporal proteome and lipidome profiles reveal hepatitis C virus-associated reprogramming of hepatocellular metabolism and bioenergetics. PLoS Pathog 6:e1000719.

Eprintsev AT, Semenova EV, Popov VN (2002) Induction of aconitate hydratase in hepatocytes of starving rats. Biochemistry (Mosc) 67:795–801.

Frodin M, Gammeltoft S (1999) Role and regulation of 90 kDa ribosomal S6 kinase (RSK) in signal transduction. Mol Cell Endocrinol 151:65–77.

Fukuda K, Takahashi K, Iwata Y, Mori N, Gonda K, Ogawa T, Osonoe K, Sato M, Ogata S, Horimoto T, Sawada T, Tashiro M, Hans A, Syan S, Crosio C, Sassone-Corsi P, Brahic M, Gonzalez-Dunia D (2001) Borna disease virus persistent infection activates mitogen-activated protein kinase and blocks neuronal differentiation of PC12 cells. J Biol Chem 276:7258–7265.

Hans A, Syan S, Crosio C, Sassone-Corsi P, Brahic M, Gonzalez-Dunia D (2001) Borna disease virus persistent infection activates mitogen-activated protein kinase and blocks neuronal differentiation of PC12 cells. J Biol Chem 276:7258–7265.

Hernanz A, de la Fuente M (1988) Characterization of aconitate hydratase from mitochondria and cytoplasm of ascites tumor cells. Biochem Cell Biol 66:792–795.

Hornig M, Briese T, Licinio J, Khabbaz RF, Altshuler LL, Potkin SG, Schwemmle M, Siemetzki U, Mintz J, Honkavuori K, Kraemer HC, Egan MF, Whybrow PC, Bunney WE, Lipkin WI (2012) Absence of evidence for bornavirus infection in schizophrenia, bipolar disorder and major depressive disorder. Mol Psychiatry 17:486–493.

Hornig M, Briese T, Lipkin WI (2003) Borna disease virus. J Neurovirol 9:259–273.

Hornig M, Solbrig M, Horscroft N, Weissenbock H, Lipkin WI (2001) Borna disease virus infection of adult and neonatal rats: models for neuropsychiatric disease. Curr Top Microbiol Immunol 253:157–177.

Huang R, Gao H, Zhang L, Jia J, Liu X, Zheng P, Ma L, Li W, Deng J, Wang X, Yang L, Wang M, Xie P (2012) Borna disease virus infection perturbs energy metabolites and amino acids in cultured human oligodendroglia cells. PLoS One 7:e44665.

Ibrahim MS, Watanabe M, Palacios JA, Kamitani W, Komoto S, Kobayashi T, Tomonaga K, Ikuta K (2002) Varied persistent life cycles of Borna disease virus in a human oligodendroglioma cell line. J Virol 76:3873–3880.

Ikuta K, Ibrahim MS, Kobayashi T, Tomonaga K (2002) Borna disease virus and infection in humans. Front Biosci 7:d470–495.

Iwata Y, Takahashi K, Peng X, Fukuda K, Ohno K, Ogawa T, Gonda K, Mori N, Niwa S, Shigeta S (1998) Detection and sequence analysis of borna disease virus p24 RNA from peripheral blood mononuclear cells of patients with mood disorders or schizophrenia and of blood donors. J Virol 72:10044–10049.

Kim YK, Kim SH, Choi SH, Ko YH, Kim L, Lee MS, Suh KY, Kwak DI, Song KJ, Lee YJ, Yanagihara R, Song JW (1999) Failure to demonstrate Borna disease virus genome in peripheral blood mononuclear cells from psychiatric patients in Korea. J Neurovirol 5:196–199.

Kurokawa M, Kornbluth S (2009) Caspases and kinases in a death grip. Cell 138:838–854.

Leong WF, Chow VT (2006) Transcriptomic and proteomic analyses of rhabdomyosarcoma cells reveal differential cellular gene expression in response to enterovirus 71 infection. Cell Microbiol 8:565–580.

Li D, Lei Y, Deng J, Zhou C, Zhang Y, Li W, Huang H, Cheng S, Zhang H, Zhang L, Huang R, Liu X, Ma L, Wang X, Li J, Xie P (2013) Human but not laboratory borna disease virus inhibits proliferation and induces apoptosis in human oligodendrocytes in vitro. PLoS One 8:e66623.

Li Q, Lau A, Morris TJ, Guo L, Fordyce CB, Stanley EF (2004) A syntaxin 1, Galpha(o), and N-type calcium channel complex at a presynaptic nerve terminal: analysis by quantitative immunocolocalization. J Neurosci 24:4070–4081.

Ludwig H, Bode L (2000) Borna disease virus: new aspects on infection, disease, diagnosis and epidemiology. Rev Sci Tech 19:259–288.

Ludwig H, Bode L, Gosztonyi G (1988) Borna disease: a persistent virus infection of the central nervous system. Prog Med Virol 35:107–151.

Matsuki T, Pramatarova A, Howell BW (2008) Reduction of Crk and CrkL expression blocks reelin-induced dendritogenesis. J Cell Sci 121:1869–1875.

Muller CF, Fatzer RS, Beck K, Vandevelde M, Zurbriggen A (1995) Studies on canine distemper virus persistence in the central nervous system. Acta Neuropathol 89:438–445.

Pearson G, Robinson F, Beers Gibson T, Xu BE, Karandikar M, Berman K, Cobb MH (2001) Mitogen-activated protein (MAP) kinase pathways: regulation and physiological functions. Endocr Rev 22:153–183.

Planz O, Pleschka S, Ludwig S (2001) MEK-specific inhibitor U0126 blocks spread of Borna disease virus in cultured cells. J Virol 75:4871–4877.

Pleschka S (2008) RNA viruses and the mitogenic Raf/MEK/ERK signal transduction cascade. Biol Chem 389:1273–1282.

Poenisch M, Burger N, Staeheli P, Bauer GvSchneider U (2009) Protein X of Borna disease virus inhibits apoptosis and promotes viral persistence in the central nervous systems of newborn-infected rats. J Virol 83:4297–4307.

Predmore ZS (2011) Exploring the effects of human cytomegalovirus infection on host cell metabolism: a proteomic approach. Doctoral dissertation, Princeton University.

Qian J, Zhai A, Kao W, Li Y, Song W, Fu Y, Chen X, Zhang Q, Wu J, Li H, Zhong Z, Ling H, Zhang F (2010) Modulation of miR-122 on persistently Borna disease virus infected human oligodendroglial cells. Antiviral Res 87:249–256.

Schneemann A, Schneider PA, Lamb RA, Lipkin WI (1995) The remarkable coding strategy of borna disease virus: a new member of the nonsegmented negative strand RNA viruses. Virology 210:1–8.

Seger R, Krebs EG (1995) The MAPK signaling cascade. FASEB J 9:726–735.

Senechal K, Halpern J, Sawyers CL (1996) The CRKL adaptor protein transforms fibroblasts and functions in transformation by the BCR-ABL oncogene. J Biol Chem 271: 23255–23261.

Šindelář L, Šindelářová M (1987) Changes in ribosephosphate isomerase and ribosephosphate pyrophosphokinase activities in tobacco infected with PVY. Biol Plant 29(6):468–472.

Suberbielle E, Stella A, Pont F, Monnet C, Mouton E, Lamouroux L, Monsarrat B, Gonzalez-Dunia D (2008) Proteomic analysis reveals selective impediment of neuronal remodeling upon Borna disease virus infection. J Virol 82:12265–12279.

Takashima M, Kuramitsu Y, Yokoyama Y, Iizuka N, Fujimoto M, Nishisaka T, Okita K, Oka M, Nakamura K (2005) Overexpression of alpha enolase in hepatitis C virus-related hepatocellular carcinoma: association with tumor progression as determined by proteomic analysis. Proteomics 5:1686–1692.

Vastag L, Koyuncu E, Grady SL, Shenk TE, Rabinowitz JD (2011) Divergent effects of human cytomegalovirus and herpes simplex virus-1 on cellular metabolism. PLoS Pathog 7:e1002124.

Williams BL, Hornig M, Yaddanapudi K, Lipkin WI (2008) Hippocampal poly(ADP-Ribose) polymerase 1 and caspase 3 activation in neonatal bornavirus infection. J Virol 82:1748–1758.

Wu YJ, Schulz H, Lin CC, Saar K, Patone G, Fischer H, Hubner N, Heimrich B, Schwemmle M (2013) Borna disease virus induced neuronal degeneration dependent on host genetic background and prevented by soluble factors. Proc Natl Acad Sci U S A 110:1899–1904.

Yang Y, Yang D, Tang G, Zhou C, Cheng K, Zhou J, Wu B, Peng Y, Liu C, Zhan Y, Chen J, Chen G, Xie P (2013) Proteomics reveals energy and glutathione metabolic dysregulation in the prefrontal cortex of a rat model of depression. Neuroscience 247:191–200.

Yeung K, Seitz T, Li S, Janosch P, McFerran B, Kaiser C, Fee F, Katsanakis KD, Rose DW, Mischak H, Sedivy JM, Kolch W (1999) Suppression of Raf-1 kinase activity and MAP kinase signalling by RKIP. Nature 401:173–177.

Zheng J, Sugrue RJ, Tang K (2011) Mass spectrometry based proteomic studies on viruses and hosts – a review. Anal Chim Acta 702:149–159.

Zhou S, Liu R, Zhao X, Huang C, Wei Y (2011) Viral proteomics: the emerging cutting-edge of virus research. Sci China Life Sci 54:502–512.

Zou W, Ke J, Zhang A, Zhou M, Liao Y, Zhu J, Zhou H, Tu J, Chen H, Jin M (2010) Proteomics analysis of differential expression of chicken brain tissue proteins in response to the neurovirulent H5N1 avian influenza virus infection. J Proteome Res 9:3789–3798.

(Accepted 6 March 2014)
(Available online 15 March 2014)